

Role of the glassy dynamics and thermal mixing in the dynamic nuclear polarization and relaxation mechanisms of pyruvic acid

M. Filibian¹, S. Colombo Serra², M. Moscardini¹, A. Rosso³, F. Tedoldi² and P. Carretta¹

¹ *University of Pavia, Department of Physics, Via Bassi 6, 27100-Pavia, Italy*

² *Centro Ricerche Bracco, Bracco Imaging Spa, via Ribes 5, 10010 Colletterto Giacosa (TO), Italy.*

³ *Université Paris-Sud, CNRS, LPTMS, UMR 8626, Orsay F-91405, France.*

The temperature dependence of ¹H and ¹³C nuclear spin-lattice relaxation rate $1/T_1$ has been studied between 4.2 K and 1.6 K in pure pyruvic acid and in pyruvic acid containing trityl radicals at a concentration of 15 mM. The temperature dependence of $1/T_1$ is found to follow a quadratic power law for both nuclei in the two samples. Remarkably that is the same temperature dependence found also for the electron spin-lattice relaxation rate in the sample containing radicals. Dynamical nuclear polarization experiments on this latter sample show that below 4 K ¹³C build up rate and $1/T_1$ scale with $1/T_{1e}$ and their values are quantitatively consistent with the presence of a thermal mixing regime between the nuclear and electron spin reservoirs. These results are explained by considering the effect of the pyruvic acid glassy dynamics on the relaxation rates and by assuming that below 4 K dynamical nuclear polarization is driven by a very good thermal contact between the nuclear and electron spin reservoirs.

I. INTRODUCTION

In recent years Dynamic Nuclear Polarization (DNP) has become one of the most intriguing and promising techniques for the nuclear spin hyperpolarization. The application of DNP has catalyzed major advances in the *in vivo* metabolic imaging of molecules labelled with low sensitivity nuclei, since it yields a dramatic enhancement of the signal to noise ratio, hardly achievable with other methods [1]. DNP increases the nuclear steady state polarization thanks to the polarization transfer from the electron to the nuclear spins under microwave irradiation close to the electron Larmor frequency (ω_e). For preclinical research purposes this phenomenon is achieved in solutions containing diamagnetic biomolecules labelled with ¹³C and a small concentration of stable radicals. The mixture is cooled down to about 1 K and, once the maximum achievable ¹³C polarization is reached, it is rapidly dissolved [2–4] and injected *in vivo* where the metabolic processes accessed by the hyperpolarized substrates are monitored by means of ¹³C Magnetic Resonance Imaging (MRI) or Spectroscopy [1, 5, 6].

While significant scientific and technological efforts are nowadays spent to introduce dissolution DNP into the clinical practice [7–9], there is a growing interest in the fundamental investigation of the physical mechanisms driving DNP. The first basic description of the DNP phenomenology dates to few decades ago [10], when different regimes, the Solid Effect, the Cross Effect and the Thermal Mixing (TM), were defined depending on the magnitude of parameters such as the nuclear resonance frequency (ω_L), the coupling among the electron and nuclear spins and the external magnetic field strength. The most common and relevant regime for the molecules utilized in metabolic imaging is seemingly the TM [2, 11, 12], which is effective when the electron spin resonance linewidth is larger than ω_L and the interactions among nuclear and electron spins are large enough to es-

tablish a common spin temperatures among the nuclear and the dipolar electron spin reservoirs.

The TM regime is attained in pyruvic acid (PA) labelled with ¹³C and doped with a concentration of trityl radicals (*c*) of the order of 10mM [12–14]. PA has been up to date the most widely investigated system for *in vivo* DNP applications due to its role in glycolytic pathways occurring in tumors [5, 6] and can be considered as a prototype system to study TM. Several DNP experiments have reported solid state ¹³C polarizations approaching 20-30 % in PA doped with trityl radicals, at a temperature $T \simeq 1.2$ K and for a magnetic field (*H*) of 3.35 Tesla [2, 5]. In order to both optimize and validate novel theoretical models of TM, several investigations of the nuclear and electron relaxation processes around 1.2 K have been performed. The effect of several parameters, including the radical concentration [12–14], the concentration of gadolinium contrast agents [12, 15] the nuclear concentration [16, 17], the amount of matrix deuteration [18], the effect of microwave saturation and the field strength [13, 14, 19], on the DNP performances of this molecule have been experimentally studied around that temperature (*T*). Remarkably very recently, the relevance of these physical quantities on DNP dynamics has also been considered in the development of novel models describing TM throughout a rate equation approach [17, 20, 21]. Nevertheless, in very few studies the role of the properties of the matrix formed by the polarized molecules and radicals has been investigated.

The importance to achieve a glassy matrix, yielding a homogeneous distribution of internuclear and electron-nuclear distances, in order to optimize DNP has been well recognized [16], but a detailed study of the lattice dynamics of the PA organic glass below 5 K and its effect on DNP has not been addressed up to date. In this regard the investigation of the nuclear spin dynamics of nuclei such as ¹H, not involved in TM, can eventually help to identify the relaxation processes involving the coupling

with the glassy dynamics.

In this manuscript we present a Nuclear Magnetic Resonance (NMR) study of PA and PA containing trityl radicals at a concentration of 15 mM utilizing both ^1H and ^{13}C nuclei. It is shown that the spin-lattice relaxation (SLR) rate of ^1H and ^{13}C nuclei and of the radical electron spins show all a nearly quadratic T dependence below 4.2 K. Remarkably, while ^1H SLR is scarcely affected by the presence of paramagnetic radicals, ^{13}C SLR shows a sizeable enhancement and a stronger T dependence. Moreover, the ^{13}C polarization build up rate is found to follow the same T dependence of the SLR times. All these results can be explained in terms of the glassy dynamics which characterizes the PA and by resorting for the DNP to the TM approach, with a very good thermal contact between the nuclear and electron spin systems below 4 K.

II. EXPERIMENTAL METHODS AND TECHNICAL ASPECTS

$1\text{-}^{13}\text{C}$ pyruvic acid (PA) and pyruvic acid (uPA) were purchased by Sigma Aldrich (Milan, Italy). The free radical trityl OX063 (tris(8-carboxyl-2,2,6,6-benzo(1,2-d:5-d)-bis(1,3)dithiole-4-yl)methyl sodium salt) was obtained from Albeda Research. For the NMR and DNP experiments 100 μL of PA and of uPA, a 15mM solution of OX063 (tris(8-carboxyl-2,2,6,6-benzo(1,2-d:5-d)-bis(1,3)dithiole-4-yl)methyl sodium salt) in 100 μL of $1\text{-}^{13}\text{C}$ pyruvic acid (PA15) and a 15mM solution of OX063 in 100 μL of unlabelled pyruvic acid (uPA15) were transferred inside quartz tubes and sonicated for 10 minutes. The samples were cooled down to 4.2 K following several procedures, detailed in Appendix A.

DNP experiments were performed by means of a homemade polarizer. A DNP-NMR probe was inserted in a bath cryostat and placed inside the bore of a superconducting magnet. Within that apparatus the temperature could be carefully controlled through helium adiabatic pumping between 1.6 K and 4.2 K. DNP was achieved by irradiating the samples with Microwaves (MW) emitted by a Gunn-diode source, mounted on the top of the probe and operating in the 96-98 GHz frequency range, with a nominal output power of 30 mW. ^1H and ^{13}C NMR probe radiofrequency (RF) circuits were tuned at 37.02 MHz and accordingly H was set to 0.87 Tesla and to 3.46 Tesla, respectively. The NMR signals were acquired with a solid-state Apollo Tecmag NMR spectrometer coupled to a homemade RF probe.

^1H NMR spin-lattice relaxation time (T_{1H}) was measured using standard saturation recovery sequences with a $\pi/2$ pulse length in the range 2 – 3 μs . In all samples ^1H recovery law was described by $y(\tau) = M_0(1 - \exp(-\tau/T_{1H}))$ (Fig. 1), indicating that all the protons undergo the same relaxation process. ^1H and ^{13}C NMR spin-spin relaxation times (T_{2H} and T_{2C}) were measured by means of the Hahn Echo sequence.

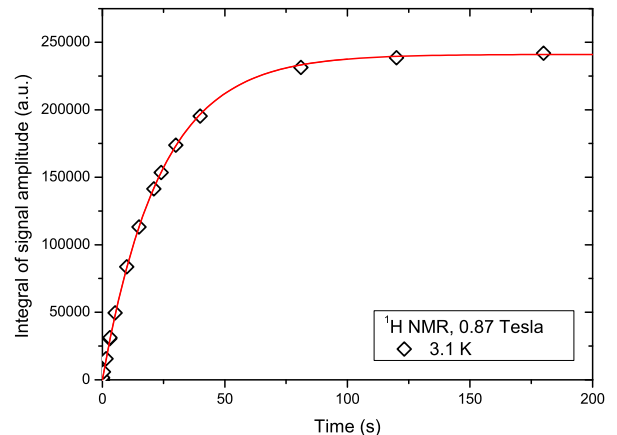


FIG. 1: Recovery law for ^1H nuclear magnetization in PA at 3.1 K and 0.87 Tesla after a saturating pulse sequence. The solid red line is the best fit according to the function $y(\tau) = M_0(1 - \exp(-\tau/T_{1H}))$.

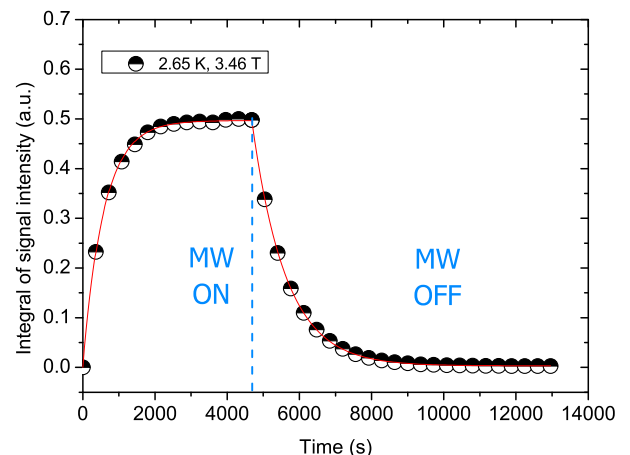


FIG. 2: ^{13}C polarization build-up under MW irradiation (MW ON) and relaxation back to the thermal equilibrium value of the nuclear magnetization (MW OFF) in PA15 at 2.67K and 3.46T. The red lines are fits according to the functions explained in the text.

DNP experiments were performed by irradiating the sample at the MW frequency maximizing the positive polarization enhancement, about 97 GHz at 3.46 Tesla. In order to acquire ^{13}C buildup curves the ^{13}C NMR signal was sampled under MW irradiation after RF saturation (Fig. 2). The Free Induction Decay (FID) signal was acquired up to steady state applying repeatedly low flip angle readout pulses (about 6°) [2] with a repetition time τ between 120 s and 600 s. ^{13}C steady state polarization

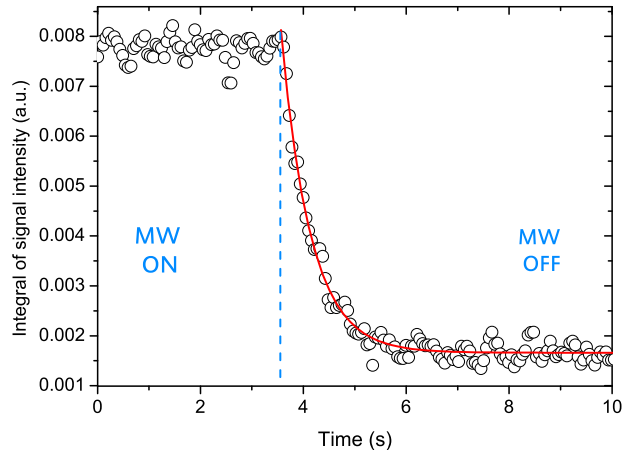


FIG. 3: Integral of the imaginary part of the ^{13}C signal as a function of time in PA15 at 2 K by means of a low flip angle acquisition scheme with $\alpha = 3^\circ$ and $\tau = 30$ ms. In this experiment the MW were switched off 3.5 seconds after the sequence start. Data have been corrected by the artificial decay induced by the application of the readout pulses. The points collected after switching off MW could be fit to a simple exponential decay $y(t) = A\exp(-t/T_{1e})$ (red curve).

$P_{N\infty}$ and the polarization time constant T_{pol} , describing the progressive growth of the polarization, were derived by fitting the build up curves to an expression that takes into account the reduction of the ^{13}C signal amplitude induced by the readout pulses [22]. In the absence of MW irradiation the same sequence could be used to measure ^{13}C T_1 (T_{1C}) by following the buildup of the ^{13}C NMR signal to the thermal equilibrium value after RF saturation. Alternatively, T_{1C} was derived from the decay of the steady state polarization to thermal equilibrium after the switch off of the MW, measured by using a low flip angle (about 6°) sequence (Fig. 2). The ^{13}C NMR signal decay was fit to the following expression

$$M(t) = M_\infty \exp\left[-\left(\frac{t}{T_{1C}} - \frac{t \log(\cos\alpha)}{\tau}\right)\right] + M_0 \quad (1)$$

with M_∞ the steady state ^{13}C magnetization under MW irradiation, α the flip angle in radians, τ the repetition time (300 s-800 s) and M_0 the ^{13}C thermal equilibrium magnetization. The logarithmic term in Eq. 1 takes into account the artificial reduction of the NMR signal induced by the readout pulses.

The electron spin-lattice relaxation time T_{1e} was derived indirectly by observing the effect of the time evolution of electron spin polarization on the NMR paramagnetic shift, and hence on the NMR signal, after the MW were turned off. In particular, after RF saturation the sample was polarized under MW irradiation for about 10-15 minutes. This time is enough for the electrons to reach steady state saturation and, additionally, to increase the

^{13}C signal-to-noise ratio significantly without having to wait the long time required to reach $P_{N\infty}$. Subsequently, a low flip angle acquisition sequence was started, with 3° flip angles and with time delay between consecutive FID acquisitions between 15 ms and 100 ms. Around 3-9 s after the beginning of the sequence, MW were switched off and the ^{13}C NMR relaxation was followed until complete ^{13}C saturation. After switching MW off, on the time scale of few seconds, the paramagnetic shift of the ^{13}C NMR line $\Delta\omega_0$ is found to vary proportionally to $P_e(t) \propto \exp(-t/T_{1e})$. The variation of $\Delta\omega_0$ correspondingly implies a modification of the shape of the NMR signal. Jóhannesson et al. [13] have described a detailed procedure which allows to analyze the NMR signal shape and to quantify the ^{13}C NMR line shift. However as long as the precise determination of the line shift is not concerned, easier approaches can be adopted to estimate T_{1e} . In this work T_{1e} was extracted by fitting the decay of the integral of the imaginary part of the ^{13}C signal $I(t)$, obtained after switching MW off, to a simple exponential decay $A\exp(-t/T_{1e})$ (Fig. 3). Further details on the procedure used to derive T_{1e} are given in Appendix B.

III. EXPERIMENTAL RESULTS

A distinct variation of the ^1H and ^{13}C SLR data was observed on changing the cooling rate of PA and PA15 below 300K. The cooling rate dependence of ^{13}C NSLR and the cooling procedures are presented in detail in Appendix A. In the following all the presented measurements were performed after flash freezing the samples in liquid helium. The T dependence of the ^1H and ^{13}C SLR rates $1/T_{1H}$ and $1/T_{1C}$, derived as explained in Section 2, are shown in Figs. 4, 5 and 6. The data in Fig. 4 and 5, measured on PA, PA15 and uPA15 by keeping ω_L of the two nuclei equal, clearly evidence that both $1/T_{1H}(T)$ and $1/T_{1C}(T)$ follow the same power law $\sim T^2$ (Table I). It is further remarked that in PA15 the prolongation of the fit curve of $1/T_{1C}(T)$ down to 1.15 K (Fig. 5) closely approaches the value reported for an equivalent sample in Ref. [12]. As regards the spin-spin relaxation times, we estimated between 1.6 and 4.2 K an almost T-independent $T_{2C} \approx 190\mu\text{s}$ and $T_{2H} \approx 35\mu\text{s}$ in PA. Also the linewidth of the NMR line was constant over the same T range, both for ^1H (30 kHz) and for ^{13}C (5.9 kHz).

In Fig.6 the comparison between $1/T_{1H}(T)$ obtained in uPA15 and uPA is depicted. One can observe that also in the radical free uPA sample $1/T_{1H}(T)$ follows a $\sim T^2$ power law and, moreover, the comparison between the two samples enlightens that the addition of 15 mM of OX063 radicals yields only a minor enhancement of $1/T_{1H}(T)$ over the explored T range ($T_{1H}(uPA15)/T_{1H}(uPA) \simeq 1.2 \div 1.3$). It is noticed that $1/T_{1H}(T)$ increases by a similar amount in the PA sample, in which also $1-^{13}\text{C}$ nuclei are present.

Remarkably, also the electron spin-lattice relaxation rate $1/T_{1e}(T)$ measured after a flash freezing procedure

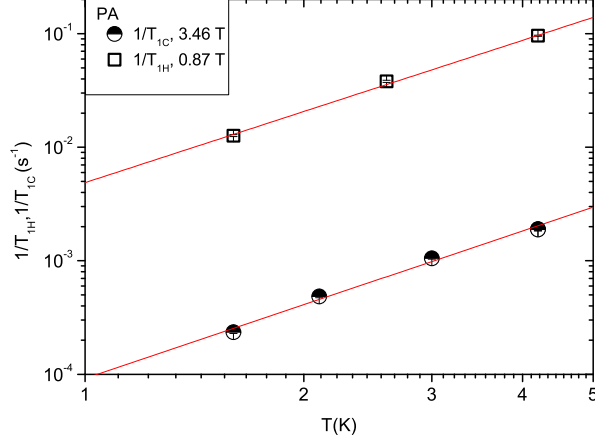


FIG. 4: Log-log plot of $1/T_{1H}(T)$ (squares) and $1/T_{1C}(T)$ (circles) in PA below 4.2 K. The red lines are fits to the power law $y(T) = aT^b$, yielding $a = 9.19 \pm 1.1 \cdot 10^{-5}$ and $b = 2.16 \pm 0.11$ for $1/T_{1C}(T)$ and $a = 4.88 \pm 0.44 \cdot 10^{-3}$ and $b = 2.08 \pm 0.07$ for $1/T_{1H}(T)$

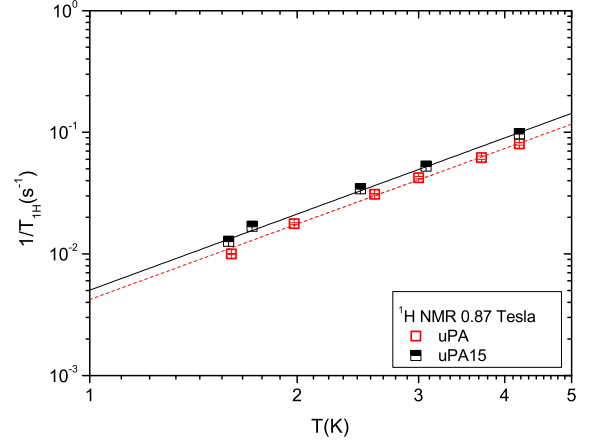


FIG. 6: Log-log plot of $1/T_{1H}(T)$ measured in uPA15 (black squares) and in uPA (red squares) below 4.2 K. Both the black and the red lines are fits to the power law $y(T) = aT^b$. The black line is the same data fit of $1/T_{1H}(T)$ in PA15 reported in Fig. 5, while the red line has been obtained with the parameters $a = 4.21 \pm 0.31 \cdot 10^{-3}$ and $b = 2.06 \pm 0.06$

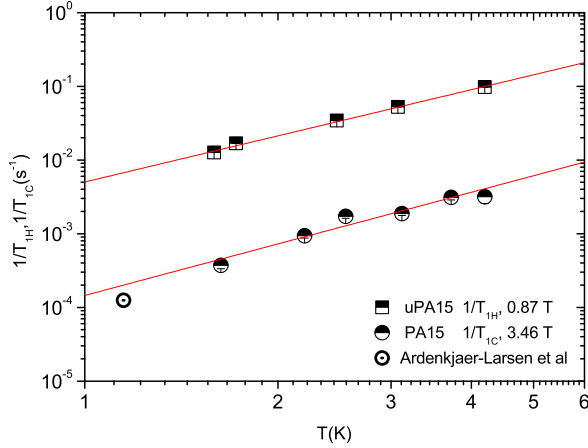


FIG. 5: Log-log plot of $1/T_{1H}(T)$ (squares) in uPA15 and of $1/T_{1C}(T)$ in PA15 (circles) below 4.2 K. The red lines are fits to the power law $y(T) = aT^b$, yielding $a = 1.45 \pm 0.46 \cdot 10^{-4}$ and $b = 2.32 \pm 0.3$ for $1/T_{1C}(T)$ and $a = 5.03 \pm 0.29 \cdot 10^{-3}$ and $b = 2.08 \pm 0.06$ for $1/T_{1H}(T)$

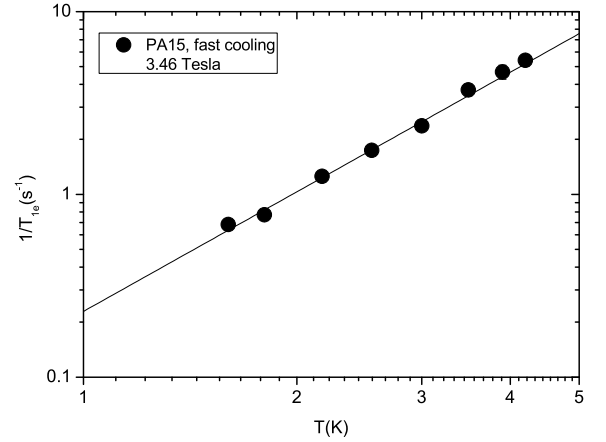


FIG. 7: Log-log plot of $1/T_{1e}(T)$ in PA15 below 4.2 K. The black lines is a fit to the power law $y(T) = aT^b$, yielding $a = 0.23 \pm 0.01 \cdot 10^{-5}$ and $b = 2.17 \pm 0.07$

(Fig. 7) could be fit to a $\sim T^2$ power law (Table I). It can be noticed that T_{1e} increases progressively upon cooling until it reaches 1.5 s around 1.6 K, a value close to the one reported in the literature at $T = 1.2$ K [12].

Now the T dependence of the two characteristic DNP parameters T_{pol} and $P_{N\infty}$ for the PA15 sample will be presented. As shown in Fig.8 $T_{pol} \sim T_{1C} \approx 400$ s around 4.2 K and grows significantly on lowering the T below 3 K, reaching values around 1500 s for $T \simeq 1.6$ K, sensibly shorter than ones of $T_{1C} \simeq 3000$ s at the same T .

Moreover, T_{pol} values at the lowest T of 1.6 K are close to the ones reported in the literature at $T \simeq 1.2$ K [14]. Also $1/T_{pol}$ follows a power law aT^b with $b \simeq 1.7$ (Table I), suggesting a common mechanism controlling that parameter, $1/T_{1H}$, $1/T_{1C}$ and $1/T_{1e}$ as a function of T . This observations definitely agree with other studies suggesting a proportionality between $T_{pol}(T)$ and $T_{1e}(T)$ [23, 24] and reporting a divergence of T_{1C} and T_{pol} (Fig.10) at very low T in several systems and in different regimes [2, 12, 13, 16, 23–28]. Nevertheless, to our knowledge the mechanism responsible for this phenomenon has not

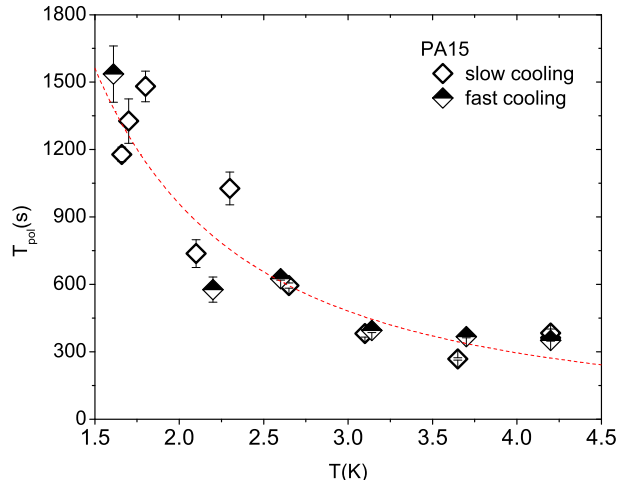


FIG. 8: T dependence of T_{pol} in PA15 below 4.2 K measured after a slow cooling (white diamonds) and a fast cooling (black and white diamonds) procedure. The dashed line is a fit according to the power law $y(T) = aT^b$, yielding $a = 3110 \pm 465$ and $b = -1.70 \pm 0.18$

been specifically addressed to date.

The values of the steady state polarization $P_{N\infty}$ for the PA15 sample, derived from the buildup curves between 1.6 K and 4.2 K are reported in Fig. 9 as a function of the inverse T ($1/T$). $P_{N\infty}$ reaches already a sizeable value, around 3-4%, at 4.2 K which raises up to 15.5 % at 1.6 K, moreover it has a linear trend at high T while, at lower T (for $1/T > 0.4 \text{ K}^{-1}$, i.e. $T < 2.5 \text{ K}$), it displays a non linear bend. These values of $P_{N\infty}$, as well the presence of the bending, cannot be explained within the traditional Borghini model [10, 29] which predicts a polarization of $\sim 80\%$ at low T and an opposite curvature for the bending. Finally note that, at variance with the NSLR data, both T_{pol} and $P_{N\infty}$ do not depend on the cooling rate.

TABLE I: Fit results of the NMR and DNP measurements according to the law $y(T) = aT^b$ in PA samples at 3.46 Tesla

Sample	Measurement	a	b
PA	$1/T_{1C}(T)$	$9.19 \pm 1.11 \times 10^{-5}$	2.16 ± 0.11
PA	$1/T_{1H}(T)$	$4.88 \pm 0.44 \times 10^{-3}$	2.08 ± 0.07
uPA	$1/T_{1H}(T)$	$4.21 \pm 0.31 \times 10^{-3}$	2.06 ± 0.06
PA15	$1/T_{1C}(T)$	$1.45 \pm 0.46 \times 10^{-4}$	2.32 ± 0.3
uPA15	$1/T_{1H}(T)$	$5.03 \pm 0.29 \times 10^{-3}$	2.08 ± 0.06
PA15	$1/T_{1e}(T)$	0.23 ± 0.01	2.17 ± 0.07
PA15	$1/T_{pol}(T)$	$3.02 \pm 0.27 \times 10^{-4}$	1.70 ± 0.18

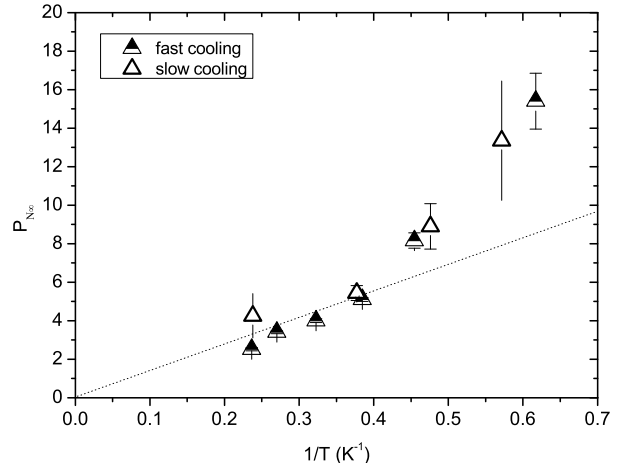


FIG. 9: $P_{N\infty}$ as a function of T in PA15 measured after a slow cooling (white triangles) and a fast cooling (black and white triangles) procedure. The error bars with caps have been estimated by the best fit of polarization buildup curves, while the error bars without caps indicate the standard deviation for a series of repeated measurements.

IV. DISCUSSION

A. Nuclear and electron spin-lattice relaxation

First the discussion of the nuclear spin-lattice relaxation (NSLR) data will be addressed. Different contributions to the NSLR can be considered, arising from the dipolar coupling with surrounding nuclei, from the hyperfine coupling with the radical electrons and due the modulation of the chemical shift tensor anisotropy (CSA). More specifically, in uPA15 and PA15 ^1H NSLR can be mainly ascribed to the fluctuations of the dipole-dipole coupling among the nuclei and of the hyperfine coupling between nuclei and radical electrons. Conversely, in uPA and PA, due to the absence of unpaired electrons, only the dipole-dipole mechanism is at work. The dipole-dipole coupling is dominated by ^1H - ^1H interaction although a minor contribution ($\sim +20\%$) from ^1H - ^{13}C is certainly present, as it is evidenced by the different ^1H SLR in the PA and uPA samples. Being the aforementioned fluctuations associated with overall independent mechanisms, the ^1H SLR in uPA15 can be expressed as

$$\frac{1}{T_{1H}} = \left(\frac{1}{T_1}\right)_{1H-1H} + \left(\frac{1}{T_1}\right)_{el} \quad (2)$$

where $(1/T_1)_{1H-1H}$ sums up the contributions from intra and intermolecular proton-proton dipolar interactions and $(1/T_1)_{el}$ is due to the hyperfine coupling between the nuclei and the radical electron spins. As it is evident from Fig. 6 the most relevant contributions to proton SLR is due to the nucleus-nucleus dipolar interaction. Accord-

ingly, in uPA the theoretical proton line broadening induced by the intramolecular couplings among the methyl protons and between the methyl and the hydroxyl proton accounts for 68% of the observed proton linewidth ($\simeq 30$ kHz), while exceeding broadening contributions can be ascribed to intermolecular ^1H - ^1H couplings. Remarkably, also in the PA sample the experimental linewidth is close to 30 kHz, which demonstrates that the line broadening due to the ^1H - ^{13}C interaction in the COOH group is negligible. Definitely, from the second moment of the proton line one can estimate a mean square amplitude of the dipolar field probed by protons $\sqrt{\langle \Delta H^2 \rangle} \simeq 7.6$ Gauss.

For ^{13}C the relevant intra and intermolecular heteronuclear dipolar interactions take place between the carboxyl ^{13}C and the methyl and hydroxyl protons. This coupling should significantly overcome the homonuclear ^{13}C - ^{13}C one, primarily because the intermolecular ^{13}C - ^{13}C distance is larger than the intramolecular ^1H - ^{13}C distance¹. Furthermore the dipolar interaction between ^1H and ^{13}C nuclei scales as $\gamma_{^1\text{H}}\gamma_{^{13}\text{C}}$, while the homonuclear one as $\gamma_{^{13}\text{C}}^2$, which is about 4 times lower. Differently from protons, the ^{13}C linewidth (5.9 kHz) cannot be explained by considering only the contribution from the ^1H - ^{13}C coupling inside the COOH group, which, according to theoretical estimates, should be of the order of 2 kHz. In fact, Macholl et al.[14] showed that in PA a sizeable CSA at the carbonyl ^{13}C site is present. Accordingly, in the case of ^{13}C SLR a further mechanism, involving the fluctuations of the chemical shift tensor, should be considered and thus, neglecting the weak homonuclear interactions, for PA15 one can write

$$\frac{1}{T_{1C}} = \left(\frac{1}{T_1}\right)_{^1\text{H}-^{13}\text{C}} + \left(\frac{1}{T_1}\right)_{\text{CSA}} + \left(\frac{1}{T_{1C}}\right)_{el} \quad (3)$$

where $(1/T_1)_{\text{CSA}}$ refers to the fluctuations of the CS tensor.

The presence of different relaxation mechanisms for ^1H and ^{13}C is supported by the observation that the ratio $T_{1C}(T)/T_{1H}(T) \simeq 53$ in PA (Fig. 4) and $T_{1C}(T)/T_{1H}(T) \simeq 39$ in PA15 (Fig. 5) results higher than the one expected if the two nuclei probed the same spectral density at the Larmor frequency $J(\omega_L)$. Infact in this case, considering

$$\frac{1}{T_1} = \frac{\gamma^2}{2} J(\omega_L) \quad (4)$$

one should have $T_{1C}(T)/T_{1H}(T) = \gamma_{^1\text{H}}^2/\gamma_{^{13}\text{C}}^2 \simeq 16$. The high ratio $T_{1C}(T)/T_{1H}(T) \simeq 53$ is consistent with the fact that the dominant dipolar contribution $(1/T_1)_{^1\text{H}-^1\text{H}}$ to $1/T_{1H}$ actually includes spectral contributions both

from one quantum (at ω_L) and double quantum transitions (at $2\omega_L$) according to [31]

$$\left(\frac{1}{T_1}\right)_{^1\text{H}-^1\text{H}} = \frac{\gamma_{^1\text{H}}^2}{2} [J(\omega_L) + J(2\omega_L)], \quad (5)$$

while

$$\left(\frac{1}{T_1}\right)_{^1\text{H}-^{13}\text{C}} = \frac{\gamma_{^{13}\text{C}}^2}{2} [J(\omega_L)] \quad (6)$$

is ruled only by one quantum transitions at ω_L . The reduction of $T_{1C}(T)/T_{1H}(T)$ in PA15 (about 30%) with respect to PA is consistent with the fact that electron-nucleus coupling yields a higher contribution to $1/T_{1C}$ than to $1/T_{1H}$. In fact, according to Table I, one observes that $T_{1C}(\text{PA})/T_{1C}(\text{PA15}) \simeq 1.6$, meaning that the hyperfine contribution to T_{1C} is about 3 times the one to T_{1H} . Since the hyperfine field generated by the electrons at the proton and carbon sites is of the same order, this can only be explained by taking into account an additional electron-nucleus relaxation mechanism probed by the ^{13}C , as it will be discussed subsequently.

The nature of the excitations leading to spin-lattice relaxation will now be analyzed. Remarkably, the common T^2 dependence of $1/T_{1H}(T)$, $1/T_{1C}(T)$ and $1/T_{1e}(T)$ strikingly points to the presence of a common source of relaxation. In particular, while NSLR is dominated by fluctuations of the dipolar interactions with the other nuclei and with the electrons, electron spin-lattice relaxation (ESLR) of the diluted radicals is rather induced by scattering with the vibrational modes. Therefore, the lattice vibrations seem to be responsible both for spatial modulation of dipolar couplings at the nuclear Larmor frequency and for the excitation of electron spin transitions at the electron Larmor frequency (ω_e). The existence of a such a broad spectral density of lattice excitations, matching both ω_L and ω_e in PA and PA15 should not surprise, since solid PA is an organic glass. These materials are characterized by a broad distribution of correlation times describing the lattice time evolution, typically ranging from 10^{-13} to 10^{-3} s or more [32, 33] even at liquid helium T. Several physical properties of glasses can be described by assuming a local lattice dynamics until very low T. In practice molecules or atoms can fluctuate among different configurations having very similar energy minima, separated by a barrier ΔE . Upon increasing T the correlation time of these lattice fluctuations can be described by an activated law $\tau_c(T) = \tau_0 \exp(\Delta E/T)$, with τ_0 the correlation time in the infinite T limit.

Then, for each activation barrier, NSLR can be simply described resorting to a spectral density of the form

$$\frac{1}{T_{1N}} = \frac{\gamma^2}{2} J(\omega_L) = \frac{\gamma^2 \langle \Delta h_{\perp}^2 \rangle}{2} \frac{2\tau_c}{1 + \omega_L^2 \tau_c^2} \quad (7)$$

where $\langle \Delta h_{\perp}^2 \rangle$ is the mean square amplitude of the random fluctuating fields probed by the nuclei in the plane perpendicular to the magnetic field. In the particular

¹ The shortest ^1H - ^{13}C distance found in the COOH group is about 1.84 Å in the most abundant pyruvic acid conformer [30] while the intermolecular ^{13}C - ^{13}C should rather be closer to 5.5 Å, equal to twice the Van Der Waals radius of the PA molecule.

condition of slow motion attained at low T, i.e. when $\omega_L \tau_c \gg 1$ the expression above reduces to

$$\frac{1}{T_{1N}} = \frac{\gamma^2 \langle \Delta h_{\perp}^2 \rangle}{\omega_L^2} \frac{1}{\tau_c} \quad (8)$$

and in this condition one would observe $1/T_{1N} \propto \tau_c^{-1} = \tau_0^{-1} \exp(-\Delta E/T)$. However, in glassy systems the presence of a broad distribution of energy barriers characterizing the dynamics causes a distribution of correlation times and accordingly a change in the T-dependence of $1/T_{1N}$. The power-law $1/T_{1N} \propto T^2$, experimentally observed in PA, could be due, for example, to a distribution of energy barriers $p(\Delta E) \propto \Delta E$. In fact, from Eq. 8 for $0 < \Delta E < \Delta E_0$, one can write

$$\begin{aligned} \frac{1}{T_{1N}} &= \int_0^{\Delta E_0} \frac{\gamma^2 \langle \Delta h_{\perp}^2 \rangle}{\omega_L^2 \tau_0} p(\Delta E) \exp(-\Delta E/T) d(\Delta E) \\ &\propto B \int_0^{\Delta E_0} \Delta E \exp(-\Delta E/T) d(\Delta E) \quad (9) \\ &= BT^2 \int_0^{\Delta E_0/T} x \exp(-x) dx \propto T^2 \text{ for } T \rightarrow 0 \end{aligned}$$

A similar result was derived also through other methods taking into account the thermally activated dynamics in asymmetric double wells characterizing the glasses [34]. Accordingly a recent implementation of the same approach has demonstrated that thermally activated dynamics of double-well systems can also explain the quadratic T dependence of $1/T_{1e}$ observed at low T in various amorphous materials, including organic glasses [35]. The validity of Eq. 9 is further corroborated by the observation that at 4.2 K $1/T_{1C}(T) \propto 1/H^2$ (unpublished results).

In other terms $1/T_1(T) \propto 1 / \langle \tau_c(T) \rangle$, where $\langle \tau_c(T) \rangle$ represents an average correlation time of the fluctuations over the distribution $p(E)$. Let us now consider the proton NSLR in uPA. Specializing $\langle \Delta h_{\perp}^2 \rangle^2$ in Eq. 8 to the case of NSLR driven by the dipolar interaction with like spins, one has [31]

$$\frac{1}{T_{1H}} = \frac{2}{5} \frac{\gamma_H^2 \hbar^2 I(I+1)}{\omega_L^2} \left\langle \frac{1}{r^6} \right\rangle \left\langle \frac{2}{\tau_c} \right\rangle \quad (10)$$

where I is the proton spin and $\langle 1/r^6 \rangle$ is the geometrical average of the inter proton distances. Considering a mean dipolar field of 7.6 Gauss, as estimated from ^1H NMR linewidth, a $\langle \tau_c \rangle \simeq AT^B$ with $A \simeq 1.5 \times 10^{-4} \text{ s/K}^B$ and $B \simeq 2.06$, is found.

A similar approach can be applied to estimate the average correlation time of the fluctuations leading to relaxation due to radicals, given by $(1/T_{1H})_{el} = (1/T_{1H})_{uPA15} - (1/T_{1H})_{uPA}$. Now one has to consider the hyperfine interaction between the protons and the neighbouring radical electron spins in a region comprised between an inner sphere having the radius of the radical $R_1 = 5.8 \text{ \AA}$, and an outer sphere with radius $R_2 = (3 * 0.74/4\pi\epsilon)^{1/3} = 26.9 \text{ \AA}$, corresponding to half of the average distance among the radicals. In this case $\langle 1/r^6 \rangle = 1/(R_1 R_2)^3$, yields an average hyperfine field of 8.2 Gauss at the ^1H site, very close to

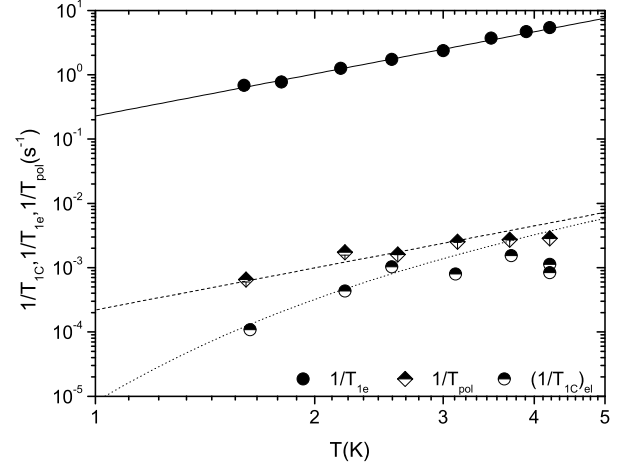


FIG. 10: Comparison among the T dependence of $1/T_{1e}$ (black dots), $1/T_{pol}$ (black and white diamonds) and $(1/T_{1C})_{el}$ (black and white circles) in PA15 below 4.2 K. The solid line is the fit of $1/T_{1e}$ according to the power law $y(T) = aT^b$, yielding the parameters reported in Tab. I. The dashed line shows the function $(N_e/N_N)1/T_{1e}$, while the dotted line gives $(N_e/N_N)1/T_{1e}(1 - P_0(T)^2)$

the one produced by the other nearby protons. Since also the NSLR enhancement associated with the radical electron spins grows as T^2 between 1.7 and 4.2 K, one estimates a characteristic fluctuation time for the magnetic field generated by the electron spins $\langle \tau_c \rangle \propto AT^B$ with $A \simeq 4.4 \times 10^{-4}$ and $B \simeq 2.16$. Remarkably, the $\langle \tau_c \rangle(T)$ describing the fluctuations leading to the relaxation term $(1/T_{1H})_{el}$ is close to the one describing the glassy dynamics probed by $(1/T_{1H})_{PA}$. Then one can conclude that in presence of radicals the ^1H relaxation involves the modulation of the field generated by the paramagnetic radicals, driven by the lattice glassy dynamics. Relaxation processes for $(1/T_{1H})_{el}$ driven by electron spin flips can be disregarded since they should be characterized by a correlation time $\langle \tau_c \rangle \ll T_{1e}$. Moreover if this was an efficient relaxation channel, one should have $(1/T_{1H}(T))_{el} \propto 1/T_{1e}(T)(1 - P_0(T)^2)$, where the last term takes into account the low T decrease of the electron spin flips due to the saturation of the equilibrium electron spin polarization P_0 . However, if this was the case $(1/T_{1H}(T))_{el}$ and $1/T_{1e}(T)$ should not follow the same quadratic law, at variance with the experimental findings.

For ^{13}C nuclei a different scenario is present. Since ^{13}C Larmor frequency is smaller than the electron spin resonance (ESR) linewidth, ^{13}C SLR can proceed also through the coupling of the ^{13}C nuclei to the electron dipolar reservoir, namely the ^{13}C and electron dipolar reservoirs are in TM. On the other hand, this is not the case for ^1H nuclei which are characterized by ω_L larger than the ESR linewidth. Within the TM process which

governs the electron-nucleus relaxation of ^{13}C one has $(1/T_{1C}(T))_{el} = 1/T_{1e}(T)(N_e/N_n)(1 - P_0(T)^2)$. The ratio N_e/N_n between the radical and ^{13}C concentrations definitely sets the order of magnitude of $(1/T_{1C}(T))_{el}$ with respect to $1/T_{1e}(T)$ and encloses a precise phenomenological meaning. The three body mechanism originating TM, involving two electron spins and one nuclear spin, can flip one of the N_n nuclear spins, as long as one of the N_e electrons relaxes to thermal equilibrium. The electron contribution to ^{13}C SLR $(1/T_{1C}(T))_{el} = (1/T_{1C}(T))_{PA15} - (1/T_{1C}(T))_{PA}$ derived from the experimental data sets is shown in Fig. 10 (black and white circles). It is remarkable to notice that below 4 K $(1/T_{1C}(T))_{el}$ data quantitatively follow the trend of the dotted function $1/T_{1e}(T)(N_e/N_n)(1 - P_0(T)^2)$, derived from the fit function of the experimental $1/T_{1e}(T)$ data (Table I), with no adjustable parameter. This is a clear evidence that indeed the ^{13}C spin ensemble and the electron dipolar reservoirs are strongly coupled in the TM, at least for $T < 4$ K. This important observation will be further supported by the T dependence of $1/T_{pol}(T)$, as it will be discussed in the following paragraph.

Before discussing the polarization parameters in PA15, some final considerations should be made on $1/T_{1e}$. The functional T dependence $1/T_{1e} \propto T^{2.2}$ has been ascribed to scattering with the glassy modes, however a sizeable dependence of the $1/T_{1e}$ magnitude on c is also expected from previous investigations [13, 14]. Even if literature data on $1/T_{1e}$ measured in different experimental setup and at different fields are contradictory [12–14, 23, 36, 37], both measurements at 1.2 K and at fixed H shown in [14] and our measurements in the 1.6–4.2 K range at higher c (unpublished data), consistently evidence the linear dependence $1/T_{1e} \propto c$ for several trityl radicals in PA. Thus, ESLR in trityl doped PA can be written as $1/T_{1e}(T) = (1/T_{1e})_g(T) + \Omega c$, where $(1/T_{1e})_g(T)$ is the term linked to the glassy dynamics and Ω is a phenomenological weakly T-dependent parameter. According to [14] $(1/T_{1e})_{(PA15)}/(1/T_{1e})_g \sim 2 \div 3$ for H=3.35 Tesla, indicating that for $c = 15$ mM the ESLR contribution due to dipole-dipole interactions among radicals, significantly overcomes the one originated by the scattering with the glassy modes, suggesting that $1/T_{1e}(T)$ should weakly depend on the cooling rate, at variance with nuclear NSLR.

Overall, from the above considerations a clear scenario emerges. In PA15 the proton NSLR processes show a T dependence which is uniquely determined by the properties of the glassy matrix. On the other hand, the dominant relaxation mechanism for ^{13}C rather involves the coupling of the nuclei to the electron dipolar reservoir through TM. Notably, due to the glassy dynamics which characterizes PA, the magnitude of T_{1C} and T_{1H} and their T dependence can possibly vary among samples containing the same radicals admixed to different molecular substrates or among samples prepared, treated and cooled with different methods, which yield to a different glassy dynamic at low T. The contribution of the glassy

modes to the ESLR can also justify some variability of T_{1e} data measured by different groups in different conditions [12–14, 23, 36, 37], even if the dominant electron-electron dipolar relaxation mechanism yields to a $1/T_{1e}(T)$ which scarcely depends on the cooling rate.

B. Dynamical nuclear polarization

As shown in Fig. 8 a nearly quadratic T dependence is found for ^{13}C $1/T_{pol}$, the DNP build up time. The most recent models describing the DNP through the thermal mixing [17, 20, 21] have stressed that the nuclear polarization under MW irradiation can be deeply influenced by several parameters such as T_{1e} , T_{ISS} , i.e. the contact time between the nuclear Zeeman reservoir and the electron dipolar reservoir, as well as by the dissipative spin diffusion among electrons and the degree of saturation by the MW. The behaviour of T_{pol} depends on the ratio T_{ISS}/T_{1e} . In particular, in presence of nuclear leakage, for $T_{ISS}/T_{1e} \sim 1$ (imperfect contact between electrons and nuclei), polarization levels much lower and T_{pol} values longer than the ones derived here are expected, both depending on T_{ISS} . On the other hand, for $T_{ISS}/T_{1e} \ll 1$, the polarization should become high and T_{pol} should shorten and depend on T_{1e} . Actually in PA15 $1/T_{pol}$ has the same T^2 dependence of $1/T_{1e}$ and its order of magnitude strikingly matches quantitatively the functional dependence of $(N_e/N_n)1/T_{1e}$ (dashed curve in Fig. 10) below 4 K. Thus, it is tempting to state that a very efficient contact is actually attained. Remarkably, below 4 K the ratio $T_{pol}(T)/T_{1C}(T)_{el}$ coincides with the function $1 - P_0(T)^2$. This can happen only if both polarization under MW irradiation and T_{1C} relaxation proceed through the same TM processes with the dipolar reservoir.

Both the polarization and the relaxation time of PA15 are consistent with the TM regime, however the experimental $P_{N\infty}$ (Fig. 9), is much smaller than the one predicted by the traditional Borghini model and a mechanism of DNP-dissipation should be identified. The dissipation inside the nuclear reservoir -via NSLR of the Carbon spins- should be irrelevant because the cooling procedure affects the value of T_{1C} of PA, but not $P_{N\infty}$. The dissipation thus should be ascribed to the electron reservoir and induced either by microwave power [21, 38] or by the presence of dissipative process in the spectral diffusion as the one discussed in [17]. At this stage we cannot discard one of the two mechanisms, or a combination of the two. Our simulations of the rate equation model introduced in [17, 20, 21] show that the bending behaviour observed in Fig. 9 is consistent with both mechanisms.

It must be recalled that, while the NSLR rates are considerably affected by the glass treatment and change upon thermal history, T_{pol} and $P_{N\infty}$ are scarcely dependent on these parameters. Since T_{1e} mainly depends on c and is only weakly dependent on the thermal history, one can attribute to the electronic relaxation channel the

leading role in determining the low-T DNP properties of PA.

Now, the quality of the electron-nucleus contact in PA seemingly evolves on raising T up to 4 K. In fact, in Fig 10 a deviation from the dotted and the dashed curves, tracing the good contact trend, is noted around $T \sim 4$ K for T_{1C} and T_{pol} . Both time constants become longer than expected, which likely indicates a substantial degradation of the electron-nucleus contact. We possibly ascribe the worsening of the electron-nucleus contact on raising T to the shortening of T_{1e} . Infact, for $T \approx 4$ K, T_{1e} is around 200 ms, a value close to the effective spin diffusion time $(N_n/N_e)T_{2C} = 190$ ms, which in turn determines the effective order of magnitude of T_{ISS} between the electron dipolar reservoir and the whole nuclear spin ensemble. Then, as explained before, for T= 4 K the threshold of the bad contact regime $T_{1e} \approx T_{ISS}$ is reached, the polarization bottleneck becomes T_{ISS} and T_{1C} and T_{pol} become longer than expected in the good contact case. On the other hand, it should be noted that in the explored T range any modulation of electron-nucleus coupling by the glassy dynamics seems definitely ineffective. Infact, since in PA15 the modulation of the electron-nucleus distances occurs over the time scales of the glassy dynamics, 10^{-5} s $<$ $\langle\tau_c\rangle$ $<$ 10^{-4} s, and considering that the magnitude of the dipolar coupling of the electron spins with the nearby nuclei Δh is such that $\gamma_{13C}\Delta h\langle\tau_c\rangle \geq 1$, the TM mixing process is marginally affected by that dynamics, in agreement with the absence of any effect of the cooling history on the DNP parameters.

Definitely one can conclude that in PA15 for $T < 4$ K TM occurs in a good contact regime where $1/T_{pol} \propto 1/T_{1e}(T)$, while for $T > 4$ K a bad contact regime is attained. The T dependence of $P_{N\infty}$ can be explained as well resorting to TM models combined with dissipative mechanisms located in the electron spin system.

V. CONCLUSIONS

It was shown that through a series of nuclear spin-lattice relaxation measurements and DNP experiments, both in pure PA and in radical doped PA, it was possible to evidence that several microscopic parameters relevant for the understanding of the dynamical nuclear polarization processes follow the same quadratic T-dependence. This trend is ascribed to the glassy dynamics which characterize the PA at low T. Finally the T dependence of the DNP build up time, of the electron contribution to ^{13}C NSLR and of the saturation polarization are found in agreement with TM regime with a very good thermal contact between the nuclear and the electron non-Zeeman reservoirs between 1.6 K and 4 K, where $1/T_{pol} \propto 1/T_{1e}(T)$. Above 4 K the TM occurs through a less efficient contact, probably due to the shortening of T_{1e} which becomes of the order of T_{ISS} . Notably, this information gives an interesting feedback to the latest theoretical developments, pointing out the relevance of

the electron spin relaxation processes, but more specifically claiming a central role for the lattice excitations in determining the ultimate DNP performances.

Appendix A: Dependence of the pyruvic acid dynamics on the cooling rate

The dependence of the experimental results on the cooling method was verified by using two different procedures: a) a slow pre-cooling inside a liquid helium bath cryostat from room T to 150 K at -0.5 K/min, followed by a rapid cooling caused by the liquid helium fill; b) a flash freezing of the samples in liquid nitrogen, followed by immersion in liquid helium. Hereafter the first method will be indicated as slow cooling (sc), while the second as fast cooling (fc). The NSLR rates showed a distinct dependence on the cooling method in both PA and in PA15 (Fig. 11). The variation of the NSLR rates is likely due to a change in the matrix dynamics properties for different cooling procedures, which is typically observed in glasses. The comparison among $1/T_{1C}(T)$ in PA and PA15, points out that upon performing a fast cooling $1/T_{1C}(T)$ doubles in PA, while it only increases by a ratio of 1.5 in PA15. The reason of this difference should be due to the additional presence in PA15 of the relaxation term $(1/T_{1C})_{el}$ due to the thermal mixing with the electrons, which is rather insensitive to the cooling rate as $1/T_{pol}(T)$.

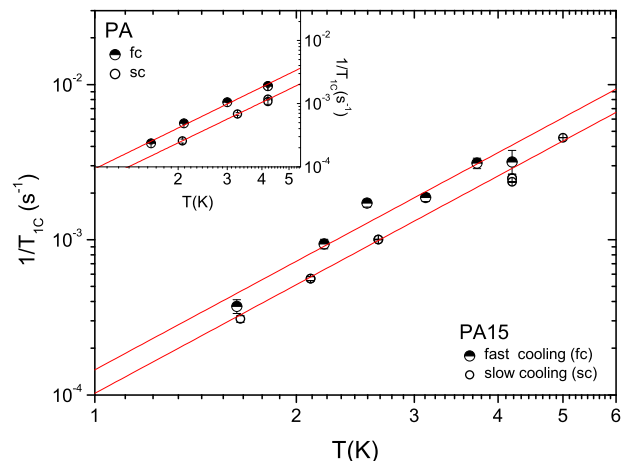


FIG. 11: Log-log plot of $1/T_{1C}(T)$ measured in PA15 after a slow cooling (white circles) and a fast cooling procedure (black and white circles) below 4.2 K. Inset: Log-log plot of $1/T_{1C}(T)$ measured in PA after a slow cooling (white circles) and a fast cooling procedure (black and white circles) below 4.2 K. The red lines are fits to the power law $y(T) = aT^b$

Appendix B: Calculation of T_{1e} from low flip angle acquisitions

As explained, it is possible to quantify T_{1e} by following the time variation of $\Delta\omega_0$. In fact, in PA15 the shift can be described by the sum $\Delta\omega_0 = \Delta M_{IS} + \Delta M_{II}$, where $\Delta M_{IS} \propto P_e$ is generated by the hyperfine coupling between the nuclei and the electrons and $\Delta M_{IS} \propto P_N$ by the dipolar nucleus-nucleus interactions [10]. Indeed, since for low radical concentration $\Delta\omega_0$ is small (300 Hz at 1.2 K in PA15 [12, 13]) its estimate from standard NMR line fits is critical. Conversely, it is rather advantageous to monitor it indirectly by analyzing the oscillations it induces in the NMR signal in the time domain.

When a line shift $\Delta\omega_0$ from the reference frequency of the NMR spectrometer ω_0 is present, having moreover the NMR signal envelope $s(t)$ and an arbitrary phase ϕ , in the domain of time (t) the imaginary component of the NMR signal $Im(t)$ has the form

$$Im(t) = x(t)\sin[(\Delta\omega_0 t) + \phi]. \quad (B1)$$

In particular, in the experiment performed to measure T_{1e} , also $\Delta\omega_0$ varies with time, but on the time scale of the whole NMR acquisition. The second time variable t' , triggered to the start of the experiment and with maximum value $N(\tau + TD)$, where TD is the time domain of the single acquisition, describes time evolution $\Delta\omega(t')$. Then Eq. B1 more properly rules as:

$$Im(t, t') = x(t)\sin[(\Delta\omega_0(t')t) + \phi], \quad (B2)$$

and its integral as

$$I(t') = \int_{\tau_1}^{\tau_2} Im(t, t') dt, \quad (B3)$$

in which the bounds τ_1 and τ_2 should be fixed in the interval in which $|s(t)|^2 \neq 0$.

In order to evaluate how T_{1e} can be correctly evaluated from $I(t')$, in this work the behaviour of $I(t')$ in Eq.B2 was simulated by means of a Python script on considering the complete shift dynamics $\Delta\omega_0(t') = \Delta M_{II}(t') + \Delta M_{IS}(t')$. The NMR signal was modelled to a Gaussian decay, with $\sigma = 105 \mu s$ and an initial signal to noise ratio equal to 500. The simulation took into account also the reduction of the signal amplitude operated by the readout pulses (Fig.12). At time \bar{t}' , when MW are switched off, for each T $P_N(\bar{t}')/P_e(\bar{t}')$ was set to the maximum value $P_{N\infty}(T)/0.5$, calculated by taking into account that $P_N(T)(\bar{t}') < P_{N\infty}(T)$ and $P_e(\bar{t}') \geq 0.5$, the value of the residual electronic polarization P_e^{res} expected for saturation at the frequency optimal for DNP [13]. For $t' > \bar{t}'$ considering both T_{1e} and T_{1N} spin-lattice relaxation processes and that P_N is reduced on increasing t' by the application of the read out pulses (see Eq. 1), the following laws were assumed to describe nuclear and electronic polarization

$$P_e(t') = (P_e^{res} - P_{E0})\exp(-t'/T_{1e}) + P_{E0} \quad (B4)$$

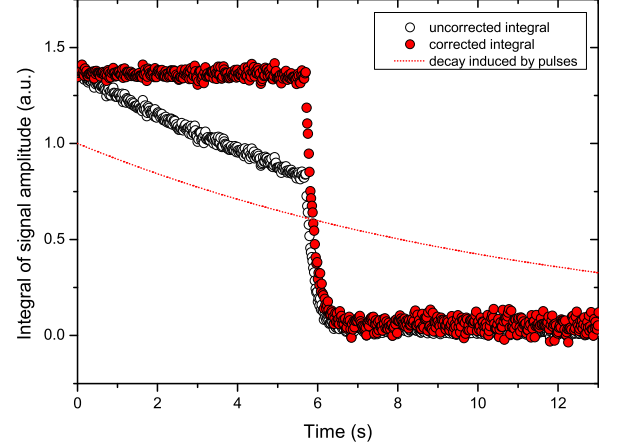


FIG. 12: Simulation of the time dependence of the integral of the imaginary signal $I(t')$ in the sequence used for the T_{1e} measurement at 4.2 K. The red dotted line shows the artificial decay induced by the read-pulses, the white circles show the uncorrected $I(t')$ as obtained by the simulation, the red circles correspond to $I(t')$ divided by the values of the red dotted line. The curves were simulated by setting $\Delta M_{IS} = 1 kHz$ and $\Delta M_{IS}/\Delta M_{II} = 10$

$$P_N(t') = (P_N(\bar{t}') - P_{N0})\exp(-t'(\frac{1}{T_{1N}} - \frac{\log(\cos(\alpha))}{\tau})) + P_{N0}, \quad (B5)$$

where P_{N0} and P_{E0} are the thermal equilibrium values for nuclear and electronic polarization respectively. In Eq. B5 T_{1N} assumed the experimental values in Fig.5, $\alpha = 3^\circ$ and τ ranged from 15 ms at 4.2 K to 100 ms at 1.8 K. Remarkably, $P_N(t')$ has an effective relaxation rate which is driven mainly by the term $\exp(t'(\log(\cos(\alpha))/\tau))$, since $1/T_{1N} \ll \log(\cos(\alpha))/\tau$, and is increased sensibly by fast repetition (12 s for $\tau = 19 ms$). Eq. B4 and B5 were used to calculate $\Delta\omega_0(t')$ and then $I(t')$. As expected, in spite of an increase of $P_N(t')/P_e(t') \simeq 0.26$ at 1.8 K, the simulation showed that imposing $T_{1e} \simeq 1 s$, $T_{1N} \simeq 1800 s$ and $\tau = 100 ms$, $I(t')$ is perfectly fit to a simple exponential decay until 60 s after t' with a decay constant of 1 s. At T=4.2 K for $T_{1e} \simeq 0.2 s$, $T_{1N} \simeq 400 s$, $\tau = 19 ms$, until 12 s after t' the simple exponential fit of $I(t')$ led to a decay constant of 0.22 s, +11 % with respect to the initial simulation parameter, only when increasing $P_N(t')/P_e(t')$ to 0.5, equal to 5 times the maximum reachable value at this T. Finally, the results didn't depend on the integration interval chosen to calculate $I(t')$.

Definitely, according to this simulation, in a time interval up to 60 s after switching off MW, one is allowed to consider strictly $\Delta\omega_0(t') = \Delta M_{IS}(t')$ and directly derive T_{1e} from the fit of $I(t')$ with a simple exponential decay. $I(t')$ obtained by the experiment was divided by the expression in Eq 1, yielding a curve properly de-

trended by the artificial decay induced by pulses(Fig.3). Eq. 1 was considered valid also for $t' < \bar{t}'$ since for $\tau \ll T_{pol}$ the buildup, occuring on times of the order of $T_{pol} \simeq 400s \div 1200s$ is overwhelmed by the fast repetition of the read out pulses. Accordingly for all Ts and $t' > \bar{t}'$, experimental data of $I(t')$ were suitably fit to a single exponential decay, after performing a smoothing procedure consisting in the unweighted averaging of 3 adjacent data points.

Appendix C: Acknowledgements

We gratefully acknowledge Albeda Research for their contributions to DNP sample preparation. This study

has been supported in part by the COST Action TD1103 (European Network for Hyperpolarization Physics and Methodology in NMR and MRI).

References

-
- [1] P. Dutta, G. V. Martinez, and R. J. Gillies, *Biophys. Rev.* **5**, 271 (2013).
- [2] J. H. Ardenkjaer-Larsen, B. Fridlund, A. Gram, G. Hansson, L. Hansson, M. H. Lerche, R. Servin, M. Thaning, and K. Golman, *PNAS* **100**, 10158 (2003).
- [3] J. Wolber, F. Ellner, B. Fridlund, A. Gram, H. Jhannesson, G. Hansson, L. Hansson, M. Lerche, S. Mnsson, R. Servin, et al., *Nuclear Instruments and Methods in Physics Research Section A: Accelerators, Spectrometers, Detectors and Associated Equipment* **526**, 173 (2004).
- [4] A. Comment, B. van den Brandt, K. Uffmann, F. Kurdzesau, S. Jannin, J. Konter, P. Hautle, W. Wenckeback, R. Gruetter, and J. van der Klink, *Concepts in Magnetic Resonance Part B: Magnetic Resonance Engineering* **31B**, 255 (2007).
- [5] K. Golman, R. in't Zandt, and M. Thaning, *PNAS* **103**, 11270 (2006).
- [6] K. Golman, R. in't Zandt, M. Lerche, R. Pehrson, and J. H. Ardenkjaer-Larsen, *Cancer Res.* **66**, 10855 (2006).
- [7] J. Kurhanewicz, D. B. Vigneron, K. Brindle, E. Y. Chekmenev, A. Comment, C. H. Cunningham, G. G. G. DeBerardinis, Ralph J, M. O. Leach, S. S. Rajan, R. R. Rizzi, et al., *Neoplasia* **13**, 81 (2011).
- [8] G. Lin and Y.-L. Chung, *Biomed Res Int.* **2014**, 625095 (2014).
- [9] O. J. Rider and D. J. Tyler, *J Cardiovasc Magn Reson.* **15**, 93 (2013).
- [10] A. Abragam and M. Goldman, *Nuclear order and disorder* (Clarendon Press, Oxford, 1982).
- [11] A. Comment, B. van den Brandt, K. Uffmann, F. Kurdzesau, S. Jannin, J. Konter, P. Hautle, W. Wenckeback, G. R., and J. van der Klink, *Magn. Res. Part B* **31B**, 255 (2007).
- [12] J. H. Ardenkjaer-Larsen, S. Macholl, and H. Johanneson, *Appl. Magn. Res.* **34**, 509 (2008).
- [13] H. Jóhannesson, S. Macholl, and J. H. Ardenkjaer-Larsen, *J. Magn. Res.* **197**, 167 (2009).
- [14] S. Macholl, H. Jóhannesson, and J. H. Ardenkjaer-Larsen, *Phys. Chem. Chem. Phys.* **12**, 5804 (2010).
- [15] L. Lumata, M. E. Merritt, C. R. Malloy, A. D. Sherry, and Z. Kovacs, *J. Phys. Chem. A* **116**, 5129 (2012).
- [16] L. Lumata, Z. Kovacs, C. Malloy, A. D. Sherry, and M. Merritt, *Phys. Med. Biol.* **56**, N85 (2011).
- [17] S. Colombo Serra, M. Filibian, P. Carretta, A. Rosso, and F. Tedoldi, *Phys. Chem. Chem. Phys.* **16**, 753 (2013).
- [18] L. Lumata, M. E. Merritt, and Z. Kovacs, *Phys.Chem.Chem.Phys.* **15**, 7032 (2013).
- [19] W. Meyer, J. Heckmann, C. Hess, E. Radtke, G. Reicherz, L. Triebwasser, and L. Wang, *Nuclear Instruments and Methods in Physics Research Section A: Accelerators, Spectrometers, Detectors and Associated Equipment* **631**, 1 (2011).
- [20] S. Colombo Serra, A. Rosso, and F. Tedoldi, *Phys. Chem. Chem. Phys.* **14**, 13299 (2012).
- [21] S. Colombo Serra, A. Rosso, and F. Tedoldi, *Phys. Chem. Chem. Phys.* p. 8416 (2013).
- [22] G. Pages and P. W. Kuchel, *Magnetic Resonance Insights* **6** (2013).
- [23] S. A. Walker, D. T. Edwards, T. A. Siaw, B. D. Armstrong, and S. Han, *Phys. Chem. Chem. Phys.* **15**, 15106 (2013).
- [24] D. Shimon, Y. Hovav, A. Feintuch, D. Goldfarb, and S. Vega, *Phys. Chem. Chem. Phys.* p. 5729?5743 (2012).
- [25] D. G. Daphna Shimon, Akiva Feintuch and S. Vega, *Phys. Chem. Chem. Phys.* **14**, 5729 (2012).
- [26] S. Jannin, A. Comment, F. Kurdzesau, J. A. Konter, P. Hautle, B. van den Brandt, and J. J. van der Klink, *J. Chem. Phys.* **128**, 241102 (2008).
- [27] F. Kurdzesau, B. van den Brandt, A. Comment, P. Hautle, S. Jannin, J. J. van der Klink, and J. A. Konter, *J. Phys. D: Appl. Phys.* **41**, 155506 (2008).
- [28] M. Plckthun, C. Bradtke, H. Dutz, R. Gehring, S. Goertz, J. Harmsen, P. Kingsberry, W. Meyer, and G. Reicherz, *Nuclear Instruments & Methods in Physics Research Section A-accelerators Spectrometers Detectors and Associated Equipment* **400**, 133 (1997).
- [29] M. Borghini, *Phys. Rev. Lett.* **20**, 419 (1968).
- [30] I. D. Reva, S. G. Stepanian, L. Adamowicz, and R. Fausto, *J. Phys. Chem. A* **105**, 4773 (2001).
- [31] A. Abragam, *Principles of Nuclear Magnetism* (Oxford University Press, 1983).
- [32] R. Böhmer, G. Diezemann, G. Hinze, and E. Rössler, *Prog. Nucl. Magn. Reson. Spectrosc.* **39**, 191 (2001).
- [33] J. Wiedersich, N. V. Surovtsev, and E. Rossler, *J. Chem. Phys.* **113**, 1143 (2000).
- [34] S. Estalji, O. Kanert, J. Steinert, H. Jain, and K. Ngai,

- Phys. Rev. B **43**, 7481 (1991).
- [35] D. Merunka, M. Kveder, and B. Rakvin, Chem. Phys. Lett. **515**, 19 (2011).
- [36] M. E. M. Lloyd Lumata and Z. Kovacs, Physical Chemistry Chemical Physics **15**, 9800 (2013).
- [37] C. Hess, J. Herick, A. Berlin, W. Meyer, and G. Reichers, Nucl. Instrum. Methods Phys. Res., Sect. A pp. 69–77 (2012).
- [38] S. Jannin, A. Comment, and J. J. Klink, Appl. Magn. Res. **43**, 59 (2012).